Full length article

Flashback propensity due to hydrogen blending in natural gas: Sensitivity to operating and geometrical parameters

Filippo Fruzza, Rachele Lamioni *, Alessandro Mariotti, Maria Vittoria Salvetti, Chiara Galletti

Dipartimento di Ingegneria Civile e Industriale, Università di Pisa, 56122 Pisa, Italy

ABSTRACT

ARTICLE INFO

Keywords:
Hydrogen
Flashback
Laminar premixed flame
Perforated burner
Decarbonization
Computational Fluid Dynamics

Hydrogen has emerged as a promising option for promoting decarbonization in various sectors by serving as a replacement for natural gas while retaining the combustion-based conversion system. However, its higher reactivity compared to natural gas introduces a significant risk of flashback. This study investigates the impact of operating and geometry parameters on flashback phenomena in multi-slit burners fed with hydrogen-methane-air mixtures. For this purpose, transient numerical simulations, which take into account conjugate heat transfer between the fluid and the solid walls, are coupled with stochastic sensitivity analysis based on Generalized Polynomial Chaos. This allows deriving comprehensive maps of flashback velocities and burner temperatures within the parameter space of hydrogen content, equivalence ratio, and slit width, using a limited number of numerical simulations. Moreover, we assess the influence of different parameters and their interactions on flashback propensity. The ranges we investigate encompass highly H_2-enriched lean mixtures, ranging from 80% to 100% H_2 by volume, with equivalence ratios ranging from 0.5 to 1.0. We also consider slit widths that are typically encountered in burners for end-user devices, ranging from 0.5 mm to 1.2 mm. The study highlights the dominant role of preferential diffusion in affecting flashback physics and propensity as parameters vary, including significant enrichment close to the burner plate due to the Soret effect. These findings hold promise for driving the design and optimization of perforated burners, enabling their safe and efficient operation in practical end-user applications.

1. Introduction

The recent EU Fit for 55 program emphasizes the urgency of reducing carbon dioxide (CO_2) emissions by 55% by 2030 compared to 1990 levels, with the ultimate goal of achieving a carbon-neutral Europe by 2050 [1]. Meeting this target necessitates a significant increase in the use of renewable energy sources to minimize reliance on fossil fuels, as outlined in the REPowEREU action [2]. The residential sector accounts for approximately 30% of final energy consumption, and by 2050, at least two-thirds of the energy demand in Europe must be fulfilled through electricity to achieve the aforementioned objectives. However, the current heating systems heavily depend on gas boilers, making the transition to electrification a costly and challenging endeavor [3]. To further accelerate decarbonization, the International Energy Agency has recommended that only zero carbon-ready gas boilers be available for sale after 2023 [4,5].

In this scenario, an interesting option is provided by hydrogen produced via water electrolysis, fed by excess wind and solar power [6]. Indeed, hydrogen can be utilized as a green energy carrier for gas boilers, employing similar technologies and minimizing the expenses

associated with heating system upgrades [7,8], as sometimes electrification is hard to achieve because of economic reasons and/or other constraints (for instance in historical buildings). Additionally, hydrogen will soon be introduced into existing gas networks at concentrations of up to 20%, enabling the storage and distribution of renewable energy through the current infrastructure [9–12] to end-user devices. Furthermore, there are expectations for the development of pipelines capable of accommodating 100% hydrogen, especially with the establishment of regionally integrated hydrogen ecosystems known as "Hydrogen Valleys", albeit this transition will require substantial efforts and occur gradually [13]. It is projected that by 2050, hydrogen, either as a hydrogen-gas mixture from the gas network or in its pure form within hydrogen valleys, could satisfy up to 18% of the energy demand for residential heating [14].

The key issue is that the replacement of natural gas with hydrogen should be accomplished safely by preserving the required performances in terms of efficiency and pollutant emissions of domestic condensing boilers. These devices typically employ premixed cylindrical or flat perforated burners, as described by Najarnikoo et al. [15], Lamioni

---

et al. [16,17], Schiro et al. [18] and Jithin et al. [19]. The burner design is well-consolidated, thanks to the extensive manufacturers' experience, for natural gas [18]. However, the physical properties of hydrogen differ strongly from those of natural gas, thus we have to understand the impact of using H_2-enriched mixtures, up to 100% H_2, on the combustion process and eventually devise modifications of the burner design. Using hydrogen can lead to excessive mixture temperatures, which may compromise the device's performance. Furthermore, the laminar flame speed of hydrogen can exceed that of natural gas by more than six times, posing challenges when utilizing hydrogen in practical applications [20] with difficulties in achieving flame stabilization. Indeed, flame stability relies on the local balance between flow velocity and flame front propagation velocity along the flame front: if the flow velocity falls below the flame front propagation velocity, the flame front moves upstream in search of a new stable configuration. However, when a stable configuration cannot be attained, the flame propagates towards the burner and upstream components, resulting in an undesired phenomenon known as flashback [21–23]. Several factors significantly contribute to flame stabilization, including flame-wall conjugate heat transfer, flow-flame interaction, curvature, stretch rate, Soret diffusion, and preferential diffusion effects [24–29]. Notably, interactions between the flame and the walls play a crucial role in the flashback dynamics. Kurdyumov et al. emphasized the influence of wall heat losses by comparing conditions with and without wall insulation [30]. Kiymaz et al. investigated the effects of wall temperature on flashback susceptibility in Bunsen-type burners, emphasizing the importance of heat transfer between the flame and the solid burner [31]. Xia et al. conducted a numerical investigation into the influence of thermal boundary conditions on boundary layer flashback in a bluff-body swirl burner using a H_2-CH_4-air mixture [32]. Additionally, the significant effect of flow-flame interactions on flashback dynamics in hydrogen-enriched swirled flames was recently emphasized by Ebi and Clemens [33] and Ranjan and Clemens [34]. These studies collectively shed light on the complex interplay between various factors and their impact on flame stabilization and flashback phenomena.

Indeed, flashback is one of the main concerns hampering the implementation of hydrogen in domestic condensing boilers. As these devices typically operate with a premixed configuration, the potential occurrence of flashback may pose hazardous situations [35]. Thus, it is crucial to carefully assess the implications of incorporating H_2 into domestic devices and develop designs that effectively prevent flashback phenomena. Recently, flashback limits of H_2-enriched mixtures in domestic boilers have been investigated experimentally evaluating the impact of wall temperature [36,37], and exploring the potential of autoignition as a mechanism for flashback initiation [38]. On the other hand, some correlations based on numerical models have been proposed to estimate the flashback velocities of hydrogen in practical configurations. Vance et al. [39] investigated the flashback limits of premixed hydrogen flames in burners with multiple slits, considering both fluid and solid regions and incorporating conjugate heat transfer in their analysis. In a recent paper from our group, we developed a transient model capable of estimating flashback limits and burner temperatures of H_2-CH_4-air mixtures in multi-slit configurations, identifying different flashback regimes depending on the hydrogen content [40]. However, a comprehensive understanding of the relative importance and interplay between the various parameters, including burner design and operating conditions, is still lacking. This comprehension is necessary for the identification of practical solutions to implement the addition of hydrogen to the gas mixture efficiently. In this perspective, this study investigates numerically the effects of various parameters on the flashback propensity of H_2-CH_4-air mixtures. We employ generalized Polynomial Chaos (gPC) expansion [41] to construct a comprehensive map of critical flashback velocities and burner temperatures. This approach allows us to explore the parameter space encompassing hydrogen content, equivalence ratio, and geometry parameters using a limited number of Computational Fluid Dynamics

(CFD) simulations. In addition, the gPC-based stochastic sensitivity analysis helps to quantitatively understand the influence of the different parameters and their interactions on the flashback propensity, assessing the relative importance of each parameter and gaining insights into their combined effects. The simulations are conducted using a 2D transient numerical model that replicates an array of slits found in real perforated burners commonly used in condensing boilers. The interpretation of the results is guided by the underlying physics governing the flashback phenomenon. We discover that preferential diffusion effects, deriving from different sources, significantly influence the flashback limits by altering the flashback physics. These effects play a crucial role and must be carefully considered to achieve a comprehensive understanding of flashback dynamics in H_2-CH_4 mixtures.

2. Numerical model

We consider a multi-slit configuration representing a section of an actual burner commonly employed in residential condensing boilers. The estimation of flashback velocity within this particular configuration is accomplished through the numerical model and procedure suggested in Fruzza et al. [40]. Taking advantage of symmetry conditions, the computational domain comprises a single infinitely-long 2D slit as shown in Fig. 1, where the solid zone corresponding to the burner is represented in black. The slit width is denoted by W, while the distance between two adjacent slits is denoted by D. The slit width is varied in the range $W \in [0.5\,\text{mm}, 1.2\,\text{mm}]$. For any variation of W, the distance between the slits D is varied to keep fixed the porosity of the burner at $W/D = 0.5$. The burner thickness is $T = 0.6$ mm for every case. The domain extends enough both downstream ($10\,\text{mm}$) and upstream ($6\,\text{mm}$) of the solid to be able to enclose the flame even in flashback conditions and hence avoid the influence of the boundary conditions on the solution. We define the *cold-flow* bulk velocity at the slit entry as

$$V_S \equiv \frac{D + W}{W} V_{in}, \tag{1}$$

where V_{in} is the uniform inlet velocity. This is the velocity we would have at the slit entry for a cold flow, i.e., neglecting the density variations of the mixture due to the high burner temperatures. By selecting a specific porosity value of $W/D = 0.5$, we maintain a consistent relationship between the inlet velocity and the slit velocity, specifically $V_S = \frac{3}{2} V_{in}$. It is important to highlight that by keeping the porosity constant, we ensure that, for a given mixture, the same V_S corresponds to the identical thermal power delivered to an ideal burner completely covered by the simulated slits.

2.1. Physical model

The problem may be described by conservation equations for mass, momentum, energy, and transport/reaction equations for the chemical species in the gas phase:

$$\frac{\partial \rho}{\partial t} + \nabla \cdot (\rho \mathbf{v}) = 0 \tag{2}$$

$$\frac{\partial}{\partial t}(\rho \mathbf{v}) + \nabla \cdot (\rho \mathbf{v}\mathbf{v}) = -\nabla p + \nabla \cdot (\bar{\tau}) \tag{3}$$

$$\frac{\partial}{\partial t}(\rho E) + \nabla \cdot (\mathbf{v}(\rho E + p)) =$$

$$= \nabla \cdot \left(k\nabla T + \sum_{j=1}^{N} h_j \left(\sum_{k=1}^{N-1} \rho D_{m,jk} \nabla Y_k + D_{T,j}\frac{\nabla T}{T} \right) \right) - \sum_{j=1}^{N} h_j \omega_j + S_{rad} \tag{4}$$

$$\frac{\partial}{\partial t}(\rho Y_i) + \nabla \cdot (\rho \mathbf{v} Y_i) = \nabla \cdot \left(\sum_{j=1}^{N-1} \rho D_{m,ij} \nabla Y_j + D_{T,i}\frac{\nabla T}{T} \right) + \omega_i, \tag{5}$$

where ρ is the density, $\mathbf{v}$ is the velocity vector, p is the pressure and $\bar{\tau}$ is the stress tensor. The ideal gas equation of state is used for the density. h_i, Y_i and ω_i are the enthalpy, the mass fraction, and the net rate of
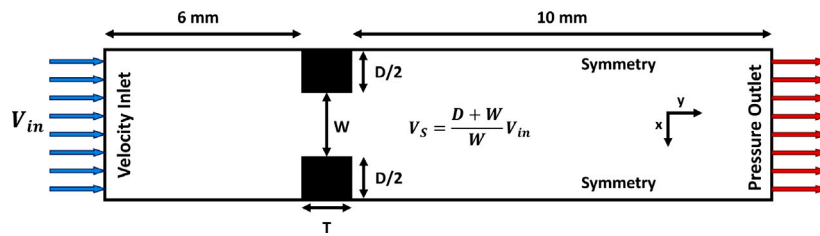
Fig. 1. Computational domain.

production of the ith species respectively, and $E = \sum_{i=1}^{N} h_i Y_i - p/\rho + \vec{v}^2/2$. k is the mass-weighted thermal conductivity of the mixture, $D_{m,ij}$ are the generalized Fick's law diffusion coefficients of the species i in species j, and $D_{T,i}$ are the thermal diffusion coefficients of the ith species. Finally, S_{rad} is the energy source associated with radiation. Inside the solid domain, we solve the energy equation:

$$\frac{\partial}{\partial t} \left(\rho_s h_s \right) = \nabla \cdot \left(k_s \nabla T \right) \tag{6}$$

where ρ_s, k_s, $c_{p,s}$, and $h_s = \int_{T_0}^{T} c_{p,s} dT$ are the density, the thermal conductivity, the specific heat, and the sensible enthalpy of the solid material. The equations are solved on a fixed structured grid, with characteristic cell size in the reaction front region of $25\,\mu m$. The grid resolution was selected to guarantee a minimum of 13 cells within the flame thickness, even in the worst-case scenario with the thinnest flame. To determine this resolution, several 1D freely-propagating flames were simulated using Cantera [42]. We selected one of these simulations as a reference, specifically a flame with 100% H_2 at $\phi = 0.8$ under the same thermodynamic conditions used in this study. By means of a grid convergence study, the solutions were proven to be well-resolved and grid-independent. We use detailed chemistry, employing the Kee-58 mechanism with 17 chemical species and 58 reversible reactions [43]. Full multi-component diffusion is modeled through the definition of generalized Fick's law coefficients derived by the Maxwell–Stefan equations [44–46]. Thermal, or Soret, diffusion is modeled using the following empirically-based composition-dependent expression provided by Kuo [47]:

$$D_{T,i} = -2.59 \times 10^{-7} T^{0.659} \left[\frac{M_i^{0.511} X_i}{\sum_{i=1}^{N} M_i^{0.511} X_i} - Y_i \right] \cdot \left[\frac{\sum_{i=1}^{N} M_i^{0.511} X_i}{\sum_{i=1}^{N} M_i^{0.489} X_i} \right], \tag{7}$$

where M_i, X_i, Y_i are the molar mass, molar fraction, and mass fraction, respectively, of the species i. Radiation is modeled by means of the gray Discrete Ordinates (DO) method [48], assuming the emissivity of the fluid-solid interface to be 0.85. The burner is modeled as a solid with the properties of the stainless steel typically used for this kind of burner, with density $\rho_s = 7719\,kg\,m^{-3}$, specific heat $c_{p,s} = 461.3\,J\,kg^{-1}\,K^{-1}$, and thermal conductivity $k_s = 22.54\,W\,m^{-1}\,K^{-1}$. The conjugate heat transfer (CHT) between the fluid and the solid zones is modeled to take account of the interaction between the flame and the burner plate. The CHT is modeled by employing Fourier's Law to calculate the heat flux across the fluid-solid interface cells [44]. It should be noted that no turbulence model is required, as all simulations exhibit fully laminar flow, with a maximum jet Reynolds number of 500.

2.2. Boundary conditions

Uniform velocity and uniform temperature of $T_u = 300\,K$ are set at the inlet, while a pressure outlet with $p = 1\,atm$ is imposed at the exit of the domain. The external edges of the domain are modeled as symmetry boundaries to take account of the interaction with the flames from the nearby slits: more specifically, we impose zero normal velocity and zero normal gradients of all variables at the symmetry plane. At the fluid-solid interfaces, a no-slip boundary condition is applied for velocity, while no thermal boundary conditions are required as heat fluxes are directly computed as described above.
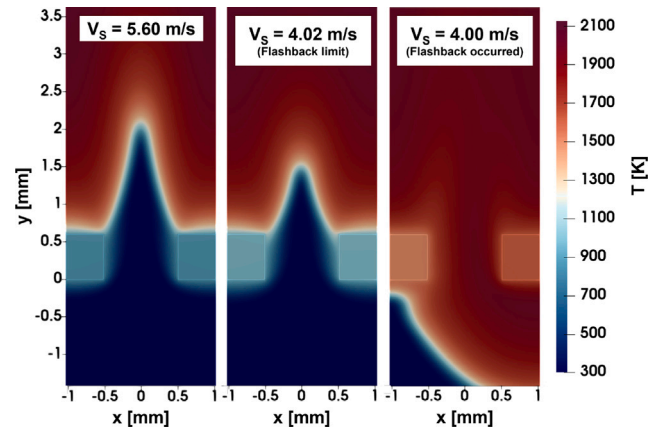
Fig. 2. Example of the procedure for the estimation of flashback velocity: snapshots of temperature field at decreasing inlet velocity for $\%H_2 = 95\%$, $\phi = 0.835$, and $W = 1\,mm$.

2.3. Estimation of flashback velocity

To assess flashback, transient simulations are performed using the pressure-based PISO algorithm available in ANSYS-FLUENT 22.1 [44]. A second-order upwind scheme is utilized for both time and space discretization. Within the fluid zone, a time step of $1\,\mu s$ is utilized. Given the significant disparity in characteristic time scales between the reactive flow in the fluid domain and the heat conduction within the solid domain, where burner temperature stabilization typically takes seconds, a time step of $1\,ms$ is employed in the solid zone to ensure computational feasibility of the simulations. The reliability of this approach has been proven in the recent study by Fruzza et al. [40], which provides further details on the methodology.

Starting from a stable flame characterized by a high inlet velocity, the inlet speed is systematically decreased, using velocity steps, until reaching a critical velocity that induces flashback. The inlet velocity steps used in this procedure are $\Delta V_{in} = 0.1\,m/s$, with an additional refinement of $\Delta V_{in} = 0.01\,m/s$ as the flashback limit is approached. This iterative procedure allows us to estimate the flashback velocity of the investigated mixture. We define the flashback velocity, V_{FB}, as the *cold-flow* bulk velocity at the slit entry, defined in Eq. (1), just before flashback occurs:

$$V_{FB} = V_S|_{FB} = \frac{D + W}{W} V_{in}|_{FB}. \tag{8}$$

A representative example of this procedure is illustrated in Fig. 2, where we plot the temperature profiles for the case with $\%H_2 = 95\%$, $\phi = 0.835$ and $W = 1\,mm$ at decreasing inlet velocities. All fuel percentage values given in this paper are expressed in terms of volume. It can be seen that, as the inlet speed is decreased, the flame approaches the hole entry and the burner temperature increases until a stable configuration is not found anymore and the flame flashes back through the slit. We note that our selection of velocity step sizes for reducing the inlet velocity ensures that this quasi-steady behavior as the flashback velocity is approached is accurately captured across all cases.

To assess the flashback propensity of a specific combination of mixture and geometry parameters, we utilize the flashback velocity scaled by the laminar flame speed of the corresponding mixture, denoted as V_{FB}/s_L. The value of s_L is determined for each mixture by analyzing 1D freely propagating flames under the corresponding thermodynamic conditions, employing Cantera [42].

3. Stochastic sensitivity analysis

In this work, a Stochastic Sensitivity Analysis is carried out, using the generalized Polynomial Chaos (gPC) method in its non-intrusive form, to investigate quantitatively how the flashback velocity, V_{FB}, its normalized value, V_{FB}/s_L, and the volume-averaged burner temperature at the flashback limit, T_B, are related to the hydrogen content, $\%H_2$, the equivalence ratio, ϕ, and the slit width, W. The aim is to obtain continuous response surfaces in the parameter space obtained for each couple of parameters, limiting the number of deterministic simulations and, at the same time, preserving a good level of accuracy of the results.

In the gPC approach, the dependence between a quantity of interest, Z, and the vector of independent uncertain parameters, ζ, is expressed by means of a polynomial expansion [41]. So, employing term-base indexing:

$$Z(\epsilon) = \sum_{j=0}^{\infty} b_j \Psi_j(\zeta(\epsilon)) \tag{9}$$

where ϵ is an aleatory event, $\Psi_j(\zeta)$ is the jth gPC polynomial and b_j is the corresponding projection coefficient. The response surface of the quantity of interest is obtained by truncating the expansion in Eq. (9) to the limit O. Applying polynomial order bounds for all one-dimensional polynomials, the truncation limit can be calculated as follows:

$$O = \prod_{k=1}^{N} (T_k + 1) - 1 \tag{10}$$

where N is the dimension of the ζ-vector, the index k identifies the particular random variable within that vector, and T_k is the maximum order of the corresponding polynomial. Finally, the coefficient b_j is defined as follows:

$$b_j = \frac{\langle Z, \Psi_j \rangle}{\langle \Psi_j, \Psi_j \rangle} = \frac{1}{\langle \Psi_j, \Psi_j \rangle} \int_\zeta Z \Psi_j \omega(\zeta) \mathrm{d}\zeta \tag{11}$$

where $\omega(\zeta)$ is the weight function connected to $\Psi_j(\zeta)$. In this paper, the integral in Eq. (11) is approximated using a Gaussian quadrature formula. The polynomial family Ψ_j has to be *a priori* defined and a suitable choice accelerates the convergence of the procedure. For the Gaussian quadrature, the optimal family is the one having a weight function analogous to the probability measure of the random variables. The choice of the polynomial family thus is related to the shape of the PDF of the uncertain parameters. In this case, since the input random variables are characterized by a uniform PDF, Legendre polynomials are selected. It is expected that, for a given variation interval of the input parameters, the uniform PDF distribution should give the largest variability of the output quantities, thus providing a 'conservative' estimation of the sensitivity to the considered input parameters. The polynomial expansion is truncated to the 3rd order in each dimension and thus, 4 quadrature points are necessary for each variable (Gauss–Legendre points).

It is worth noting that the UQ analysis could be performed by considering the three parameters, i.e., H_2 content, equivalence ratio ϕ, and slit width W, all together, resulting in 64 simulation points. However, we decided to carry out three different stochastic sensitivity analyses for each couple of parameters keeping the third one fixed. This leads to 16 simulations for each analysis and, thus, to a total of 48. The gain in computational effort is not negligible, as each simulation point implies a number of transient numerical simulations to observe flashback. Moreover, by considering the 3 parameters together, for

Table 1
Quadrature points for the two input parameters: H_2 content and equivalence ratio.

Quadrature points	1st	2nd	3rd	4th
H_2 content [%]	86.0	89.9	95.0	98.9
ϕ [–]	0.535	0.665	0.835	0.965

Table 2
Quadrature points for the two input parameters: H_2 content and slit width.

Quadrature points	1st	2nd	3rd	4th
H_2 content [%]	81.4	86.6	93.4	98.6
W [mm]	0.55	0.73	0.97	1.15

Table 3
Quadrature points for the two input parameters: equivalence ratio and slit width.

Quadrature points	1st	2nd	3rd	4th
ϕ [–]	0.535	0.665	0.835	0.965
W [mm]	0.55	0.73	0.97	1.15

some combinations of the values, flashback does not occur, and this would introduce possible discontinuities in the response surfaces that cannot be analyzed by the gPC approach. Conversely, by varying only two parameters, this can be avoided by ad-hoc tailoring the ranges of variation. Indeed, in each analysis, the ranges of the considered parameters are selected to encompass the broadest possible region within the parameter space where flashback phenomena can occur. For the $\%H_2/\phi$ analysis, we use $\%H_2 \in [85\%, 100\%]$ and $\phi \in [0.5, 1.0]$, with $W = 1\,\mathrm{mm}$. For the $\%H_2/W$ analysis, we use $\%H_2 \in [80\%, 100\%]$ and $W \in [0.5\,\mathrm{mm}, 1.2\,\mathrm{mm}]$, with $\phi = 0.7$. Finally, for the ϕ/W analysis, we use $\phi \in [0.5, 1.0]$ and $W \in [0.5\,\mathrm{mm}, 1.2\,\mathrm{mm}]$, with $\%H_2 = 100\%$. Outside of this region, specifically when reducing the values of ϕ, H_2 content, or W while keeping the remaining parameters constant, a decrease in input velocity leads to flame quenching instead of flashback. Consequently, it becomes impossible to define a flashback velocity in such cases. The quadrature points, i.e. the values of the parameters at which the computations are carried out, are reported in Tables 1, 2, and 3 for each considered analysis.

In addition, two independent simulations are performed for each analysis to test the reliability of the response surfaces. These test points are chosen a posteriori to be distant from each other and from the quadrature points, placed in opposite regions of the parameter space. The variability of the output quantities is described in terms of total variance as $\sigma^2 = \sum_{j=1} (b_j^*)^2$, with $b_j^* = b_j |\Psi_j|$, $|\Psi_j|$ being the norm of the jth polynomial. The sensitivity of the quantities of interest to a single input parameter or to a combination of them is computed using the variance decomposition method proposed by [49]. The Sobol' index (also called sensitivity index) I_i is defined as the ratio between the partial variance σ_i^2, i.e., the variance only due to the ith uncertain input parameter, and the total variance σ^2, as $I_i = \sigma_i^2/\sigma^2$. In the case of a two-parameter analysis, the Sobol' index relative to the interaction between the two parameters is equal to $I_{1,2} = 1 - I_1 - I_2$.

4. Results

4.1. Effect of H_2 content and equivalence ratio

The sensitivity analysis of the flashback velocity, V_{FB}, its normalized value, V_{FB}/s_L, and the burner plate temperature at the flashback limit, T_B, is performed as the H_2 content and the equivalence ratio vary in the ranges $\%H_2 \in [85\%, 100\%]$ and $\phi \in [0.5, 1.0]$. The slit width is fixed at $W = 1\,\mathrm{mm}$, which is chosen to ensure a sufficiently large area in the parameter space for defining the flashback velocity. It is important to emphasize that when lowering ϕ while keeping the H_2 content at 85%, or when reducing the H_2 content while maintaining $\phi = 0.5$, we observe flame quenching for low inlet velocity, making it
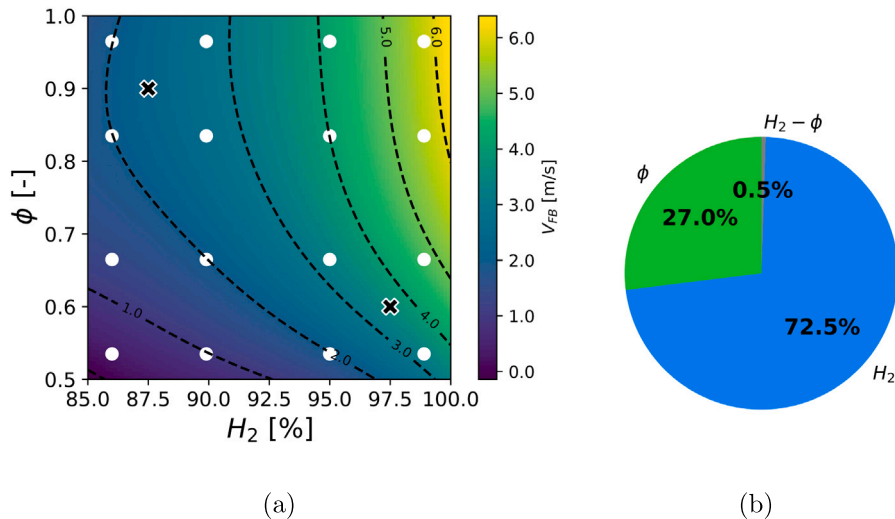
Fig. 3. (a) Stochastic response surface of V_{FB} in the %H_2 - ϕ parameter space. White dots represent quadrature points. Black crosses indicate test points. (b) Sobol' indices. (For interpretation of the references to color in this figure legend, the reader is referred to the web version of this article.)
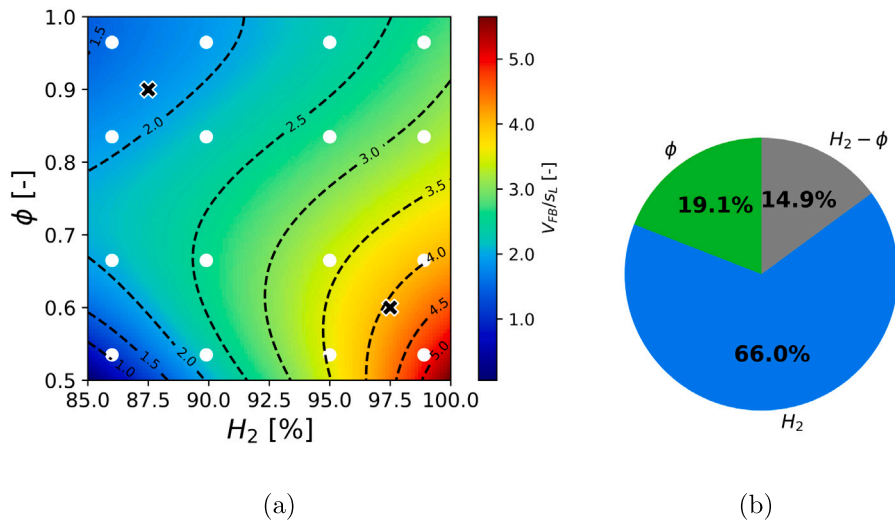

Fig. 4. (a) Stochastic response surface of V_{FB}/s_L in the %H_2 - ϕ parameter space. White dots represent quadrature points. Black crosses indicate test points. (b) Sobol' indices. (For interpretation of the references to color in this figure legend, the reader is referred to the web version of this article.)

impossible to define a flashback velocity in those cases. After obtaining the response surfaces, two test simulations are conducted for the points with %$H2$ = 87.5% and ϕ = 0.9, as well as %$H2$ = 97.5% and ϕ = 0.6. The results for both V_{FB} and T_B are found to be consistent with the response surface values at these points, with an error of less than 2%.

Flashback velocity. Fig. 3 shows the flashback velocity V_{FB} as a colored map in the H_2 content - ϕ space, with the relative Sobol' indices given as percentages. We observe that V_{FB} ranges from $0.2\,\mathrm{m/s}$, for low %H_2 and low ϕ, to $6\,\mathrm{m/s}$, for high %H_2 and high ϕ. The dominant input parameter influencing V_{FB} is the hydrogen content, with a Sobol' index of I_{H_2} = 72.6%. There is also a weaker but still significant dependence on the equivalence ratio (ϕ), with a Sobol' index of I_ϕ = 26.9%. Interestingly, the sensitivity of V_{FB} to these two parameters is consistent across the entire parameter space, as indicated by the interaction Sobol' index $I_{H_2,\phi}$ being close to zero.

The trend of V_{FB} in the parameter space, which shows an increase in flashback velocity with increasing hydrogen content and equivalence ratio independently, mimics the well-known trend of the laminar flame speed s_L. To better understand the flashback physics, it is more appropriate to consider the V_{FB}/s_L ratio. Indeed, this normalization

eliminates the trivial dependence on the variability of s_L and allows for a clearer assessment of the differences in the flashback phenomena.

Normalized flashback velocity. Fig. 4 shows the V_{FB}/s_L map in the parameter space and the relative Sobol' indices. The variation of the normalized flashback velocity over the parameter space is significant, ranging from $V_{FB}/s_L \lesssim 1.0$ to $V_{FB}/s_L \gtrsim 5.0$. The minimum is observed in the region with low H_2 content and low equivalence ratio, very close to the quenching limit, probably due to the low reactivity of the mixture. The maximum is observed in the region with high H_2 content and low equivalence ratio. The hydrogen content is the most influential parameter, with I_{H_2} being 66.0%, while the equivalence ratio contributes to 19.1% of the variability. Moreover, as confirmed by the interaction Sobol' index $I_{H_2,\phi}$ = 14.9%, we observe a larger impact of ϕ for high H_2 contents, with the maximum V_{FB}/s_L occurring in the zone with the highest H_2 content and the lowest equivalence ratio.

As previously mentioned, the ratio V_{FB}/s_L is the most effective parameter for assessing flashback propensity, as it highlights the differences in the flashback phenomena, eliminating the trivial dependence on the value of the laminar flame speed. To visualize and better
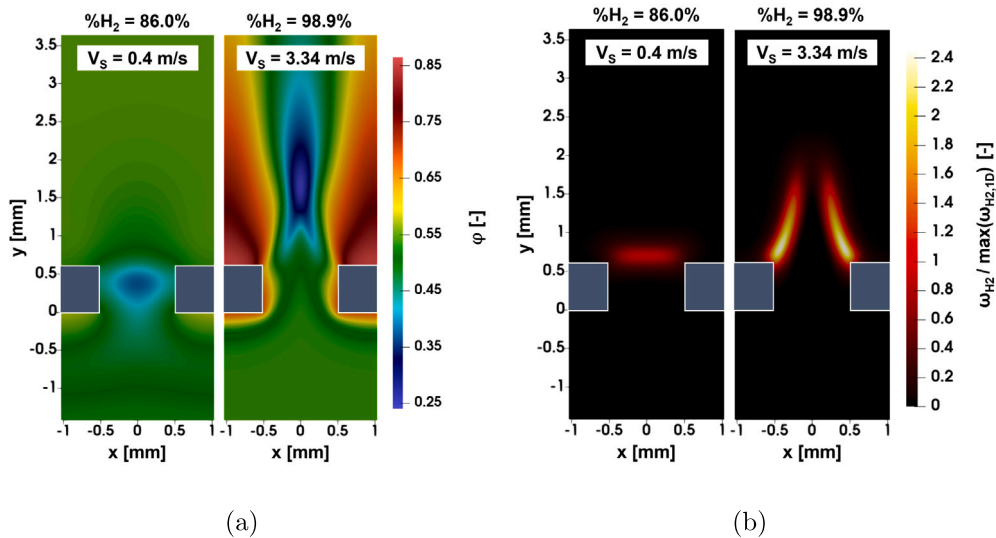
Fig. 5. (a) Local equivalence ratio for flashback limit cases with %H$_2$ = 86% and %H$_2$ = 98.9% at ϕ = 0.535. (b) Normalized molecular hydrogen consumption rate for flashback limit cases with %H$_2$ = 86% and %H$_2$ = 98.9% at ϕ = 0.535. (For interpretation of the references to color in this figure legend, the reader is referred to the web version of this article.)
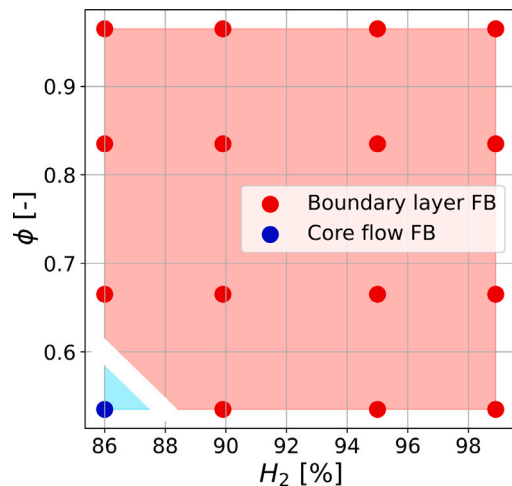

Fig. 6. Flashback regimes in the %H$_2$ - ϕ parameter space. Blue represents "core flow flashback", and red represents "boundary layer flashback". (For interpretation of the references to color in this figure legend, the reader is referred to the web version of this article.)

understand the underlying physics, Fig. 5 presents the local equivalence ratio, φ, and the normalized molecular H$_2$ consumption rate, $\omega_{H_2}/\max(\omega_{H_2,1D})$, for the flashback limits of the cases with %H$_2$ = 86.0% and %H$_2$ = 98.9% at ϕ = 0.535. $\max(\omega_{H_2,1D})$ is the maximum H$_2$ consumption rate obtained in the corresponding 1D flame. Following Pope et al. [50], the local equivalence ratio φ is defined by:

$$\varphi = \frac{2 \chi_C + 1/2 \chi_H}{\chi_O}; \quad \chi_l = \sum_{k=1}^{N_{sp}} a_{k,l} X_k, \quad (12)$$

where χ_l denotes the mole fraction of element l, X_k is the mole fraction of species k, and $a_{k,l}$ is the number of atoms of element l contained in a molecule of species k. It is important to note that, since the unburnt mixture is homogeneous, variations in the local equivalence ratio can only arise due to preferential diffusion. The snapshots are obtained from simulations performed at the corresponding quadrature points and depict the flashback limit, i.e., the last stable flame before the occurrence of flashback. We observe that the hydrogen content has a significant influence on the effect of preferential diffusion on the local

equivalence ratio, leading to a local enrichment of up to φ = 0.86 in the flame base zone for the case with 98.9% H$_2$. In addition to preferential diffusion effects caused by curvature, typically occurring in mixtures with $Le < 1$, we observe Soret-induced preferential diffusion effects. As shown by Vance et al. [27], since the Soret coefficients of light species like H$_2$ and CH$_4$ are negative (diffusion from cold to hot regions), while heavier species like O$_2$ have positive Soret coefficients (diffusion from hot to cold regions), a higher φ is observed in close proximity to the hot surfaces, where temperature gradients are high. The local enrichment induced by both sources of preferential diffusion intensifies the flame in the flame base region, resulting in an increased flame speed in the presence of high velocity gradients near the wall. This effect favors flashback by modifying s_L in the critical region, thus leading to a higher value of V_{FB}/s_L. In such cases, we observe flashback occurring asymmetrically at the burner wall. For the cases with lower hydrogen (H$_2$) content, preferential diffusion effects do not play a significant role. When the inlet velocity is decreased, flashback occurs smoothly in this case, with the flame front moving towards the slit entry, flattening, heating up the burner, and then passing through the slit symmetrically. We refer to these two distinct flashback regimes as the "boundary layer flashback" regime and the "core flow flashback" regime, respectively [40]. In Fig. 6, we partition the parameter space into two regions corresponding to the two flashback regimes based on observations derived from transient simulations conducted at the quadrature points. It can be observed that, for the selected parameter set, the prevalence of the "boundary layer flashback" is evident, with this phenomenon occurring at all quadrature points except for the one characterized by lower %H$_2$ and ϕ, where "core flow flashback" is observed instead. It is worth noting that the transition between these two flashback regimes corresponds to values of V_{FB}/s_L between 1 and 2, as already observed in Fruzza et al. [40].

The role of preferential diffusion in promoting flashback explains why the higher values of V_{FB}/s_L are observed in the parameter space region characterized by the highest %H$_2$ and the lowest ϕ, where the influence of preferential diffusion effects is expected to be more pronounced.

Burner temperature. Fig. 7 shows the burner plate temperature at the flashback limit, which represents the maximum attainable temperature of the burner, in the parameter space, and the relative Sobol' indices. We observe a significant variation in the maximum temperature of the burner plate within the investigated parameter space. The minimum,
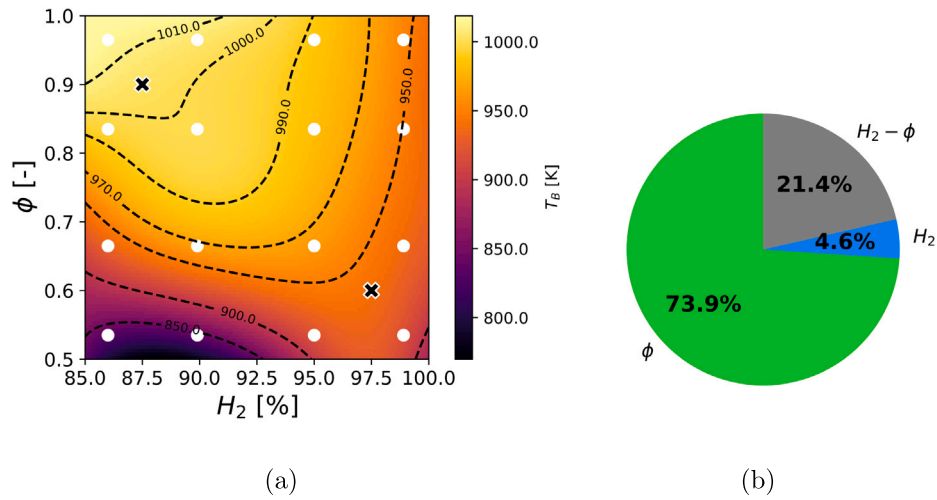
(a)

(b)

Fig. 7. (a) Stochastic response surface of T_B in the %H$_2$ - ϕ parameter space. White dots represent quadrature points. Black crosses indicate test points. (b) Sobol' indices. (For interpretation of the references to color in this figure legend, the reader is referred to the web version of this article.)
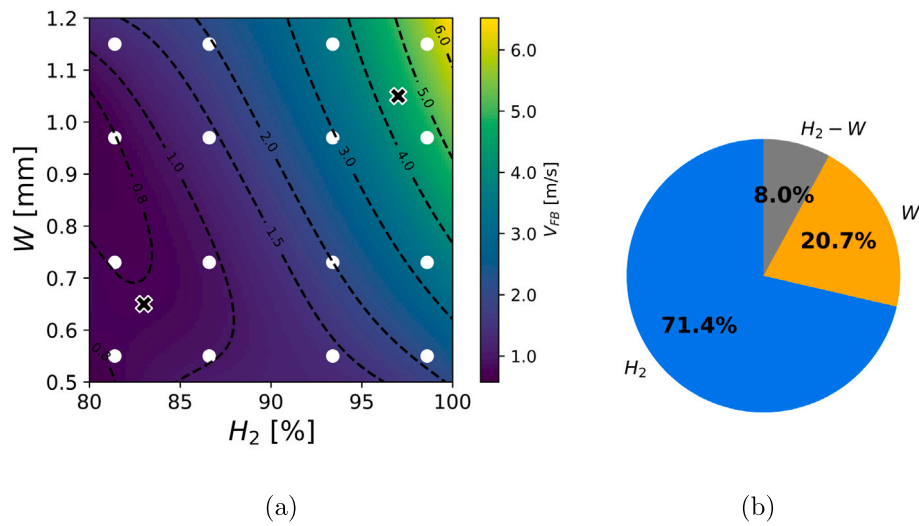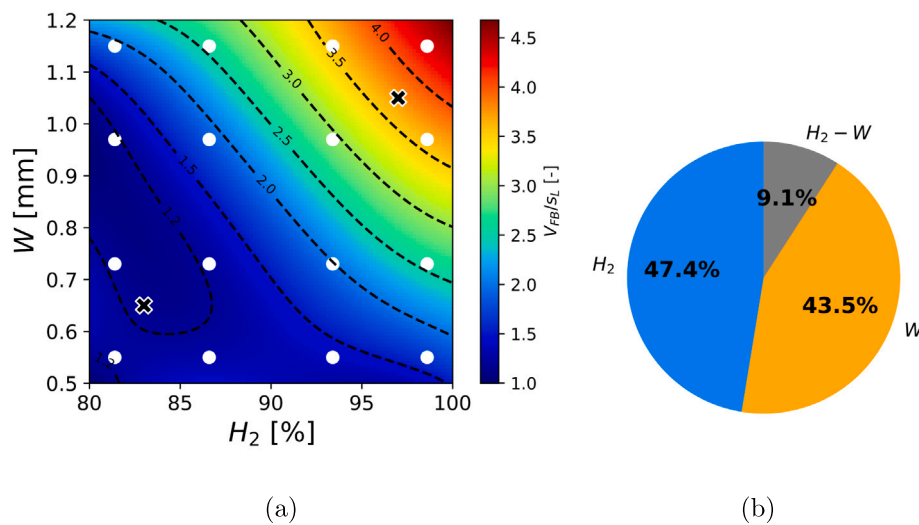

(a)

(b)

Fig. 8. (a) Stochastic response surface of V_{FB} in the %H$_2$ - W parameter space. White dots represent quadrature points. Black crosses indicate test points. (b) Sobol' indices. (For interpretation of the references to color in this figure legend, the reader is referred to the web version of this article.)
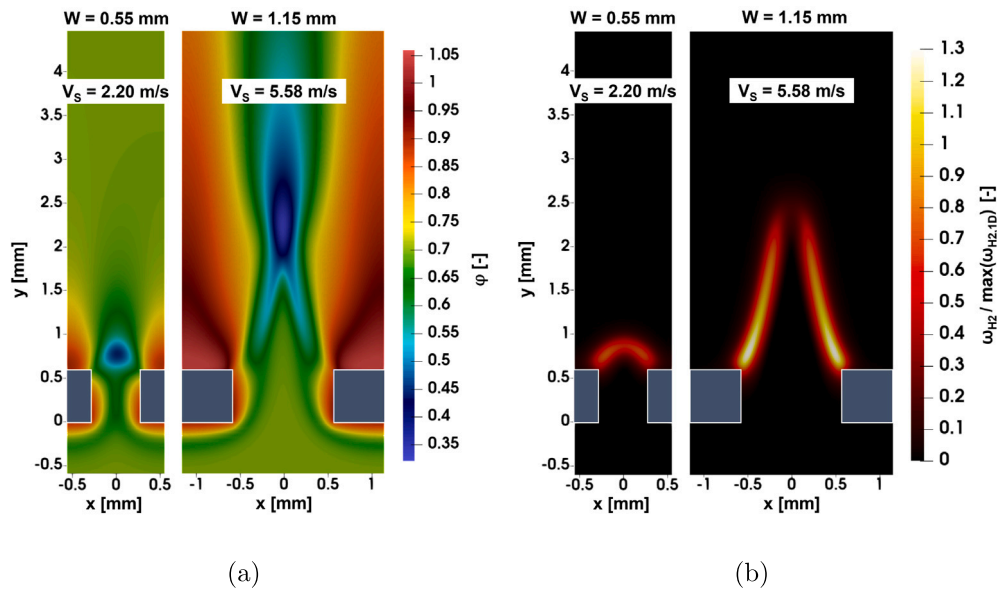

(a)

(b)

Fig. 9. (a) Stochastic response surface of V_{FB}/s_L in the %H$_2$ - W parameter space. White dots represent quadrature points. Black crosses indicate test points. (b) Sobol' indices. (For interpretation of the references to color in this figure legend, the reader is referred to the web version of this article.)

Fig. 10. (a) Local equivalence ratio for flashback limit cases for $W = 0.55\,\text{mm}$ and $W = 1.15\,\text{mm}$ with $\%H_2 = 98.9\%$ and $\phi = 0.7$. (b) Normalized molecular hydrogen consumption rate for $W = 0.55\,\text{mm}$ and $W = 1.15\,\text{mm}$ with $\%H_2 = 98.9\%$ and $\phi = 0.7$. (For interpretation of the references to color in this figure legend, the reader is referred to the web version of this article.)

$T_B \approx 825\,\text{K}$, is observed for low H_2 content and low equivalence ratio, while the maximum, $T_B \approx 1010\,\text{K}$, is observed for low H_2 content and high equivalence ratio. In most of the parameter space, the variability of T_B is primarily attributed to changes in ϕ. This is supported by the Sobol' indices, $I_\phi = 74.0\%$ and $I_{H_2} = 4.6\%$. However, as the hydrogen content approaches 100%, T_B becomes almost independent of ϕ, with $T_B \approx 950\,\text{K}$ for all equivalence ratios. The difference in the sensitivity of T_B to ϕ in different regions of the parameter space is quantified by the interaction Sobol' index $I_{H_2,\phi} = 21.4\%$.

The variability of T_B in the parameter space can be attributed to various factors, including the position of the flame at the flashback limit, the total mass flow rate, radiative losses, the flame attachment to the burner plate, and the contact area between the hot burnt gases and the top surface of the burner plate. Due to the complexity of heat exchange phenomena between the flame, burner, and external environment, understanding and predicting the interplay of these effects is challenging. Therefore, the construction of a map in the parameter space using the gPC and the Stochastic Sensitivity Analysis provide a valuable approach for qualitatively predicting the maximum burner temperature when varying the parameters of interest.

4.2. Effect of H_2 content and slit width

A similar analysis is conducted by varying the H_2 content in the range $\%H_2 \in [80\%, 100\%]$ and the slit width in the range $W \in [0.5\,\text{mm}, 1.2\,\text{mm}]$, while keeping a constant equivalence ratio of $\phi = 0.7$. This specific value of ϕ is chosen to enable the definition of a flashback velocity throughout the entire parameter space, while ensuring the mixtures remain sufficiently lean, aligning with practical considerations. Two test simulations are carried out at the points with $\%H2 = 83\%$ and $W = 0.65\,\text{mm}$, and $\%H2 = 97\%$ and $W = 1.05\,\text{mm}$: the results for both V_{FB} and T_B are found to be consistent with the response surface with an error of less than 1%.

Flashback velocity. Fig. 8 illustrates the relationship between the flashback velocity and the two input parameters, as well as the corresponding Sobol' indices. The flashback velocity demonstrates significant variability across the entire parameter space, with the maximum value, $V_{FB,\text{max}} \simeq 6.1\,\text{m/s}$, being nearly ten times larger than the minimum, $V_{FB,\text{min}} \simeq 0.7\,\text{m/s}$. The variation of V_{FB} is primarily influenced by the
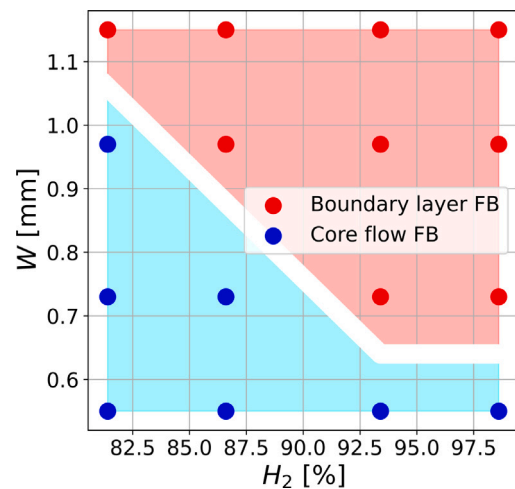

Fig. 11. Flashback regimes in the $\%H_2$ - W parameter space. Blue represents "core flow flashback", and red represents "boundary layer flashback". (For interpretation of the references to color in this figure legend, the reader is referred to the web version of this article.)

H_2 content, with a Sobol' index of $I_{H_2} = 71.4\%$. However, the slit width also exhibits a non-negligible impact on V_{FB}, being $I_W = 20.7\%$, but only for high H_2 contents, at which we observe the flashback velocity ranging from $V_{FB} \simeq 2.3\,\text{m/s}$ to $V_{FB} \simeq 6.1\,\text{m/s}$.

The underlying physical reasons for the non-negligible dependence of V_{FB} on the W are not straightforward. Once again, analyzing the variation of the normalized value V_{FB}/s_L provides a better approach to understanding the involved phenomena.

Normalized flashback velocity. Fig. 9 illustrates V_{FB}/s_L in the parameter space and the corresponding Sobol' indices. The scaled flashback velocity exhibits a significant variability of approximately 450% across the parameter space, ranging from 1 to 4.5. Interestingly, the dependence of V_{FB}/s_L on W is equally important as the dependence on $\%H_2$, as indicated by the similar values of their respective Sobol' indices, $I_W = 43.5\%$ and $I_{H_2} = 47.4\%$.
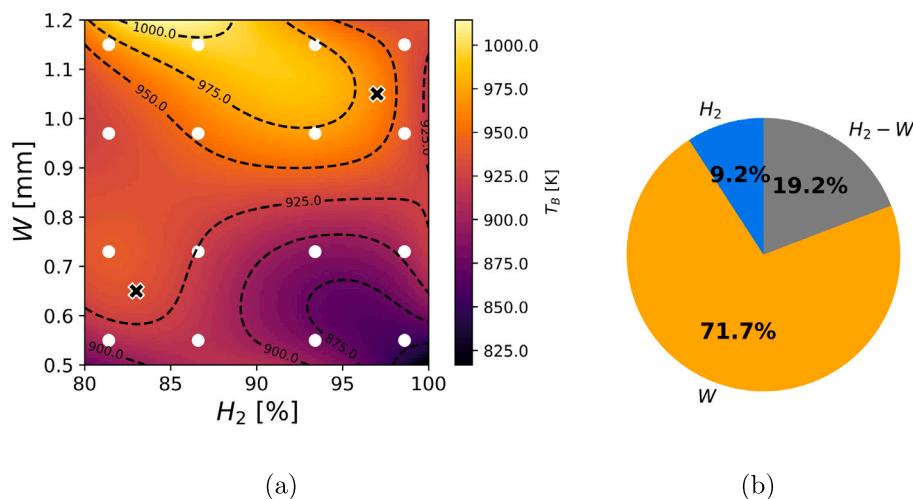
Fig. 12. (a) Stochastic response surface of T_B in the %H_2 - W parameter space. White dots represent quadrature points. Black crosses indicate test points. (b) Sobol' indices. (For interpretation of the references to color in this figure legend, the reader is referred to the web version of this article.)
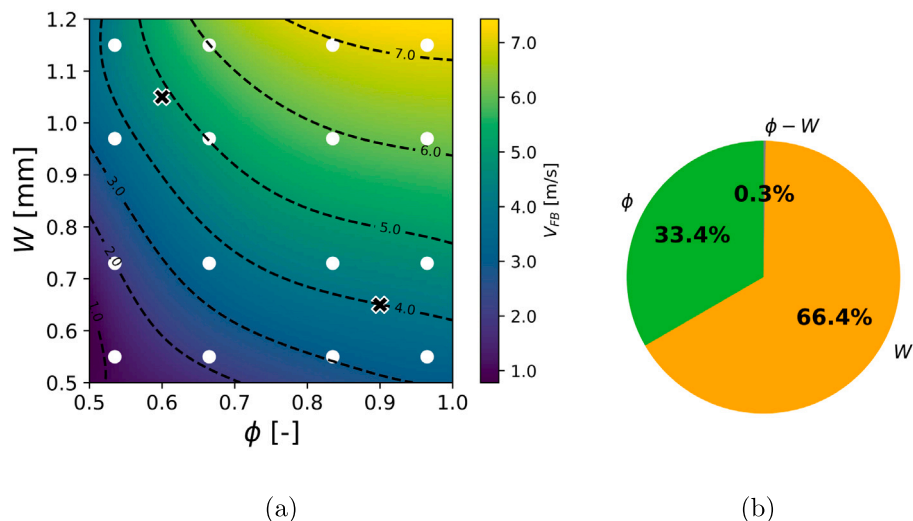

Fig. 13. (a) Stochastic response surface of V_{FB} in the ϕ - W parameter space. White dots represent quadrature points. Black crosses indicate test points. (b) Sobol' indices.

These results indicate that the slit width plays a crucial role in the physics of flame stabilization. At the same time, the substantial variability observed in V_{FB}/s_L for high H_2 contents suggests a significant influence of preferential diffusion effects. Fig. 10 shows the local equivalence ratio, φ, and the normalized molecular H_2 consumption rate, $\omega_{H_2}/\max(\omega_{H_2,1D})$, for the flashback limits of two cases with different slit widths, $W = 0.55\,\text{mm}$ and $W = 1.15\,\text{mm}$, and the same mixture, %$H_2 = 98.9\%$ and $\phi = 0.7$. In the case of narrow slits, where the width is comparable to the flame thickness, the formation of highly curved flame front structures is limited, resulting in relatively weak preferential diffusion effects. Furthermore, the presence of low temperature gradients due to a uniform flow temperature at the slit exit suppresses Soret-induced preferential diffusion effects. On the other hand, wider slits with higher inlet velocities facilitate the development of highly curved flame fronts, leading to stronger preferential diffusion effects. Additionally, wider slits exhibit higher temperature gradients at the slit exit, promoting greater Soret-induced preferential diffusion effects in the flame base region. These combined effects contribute to a higher flashback velocity by enhancing the flame speed in the critical region close to the walls. In Fig. 11, we show the parameter space divided into two regions corresponding to the two flashback regimes described above. It is evident that both parameters affect the flashback

dynamics. We observe "core flow flashback" in regions characterized by low values of %H_2 and W, while "boundary layer flashback" occurs in regions with high %H_2 and W. Furthermore, upon comparison with the plot in Fig. 9, we observe that the boundary between these two regimes coincides with V_{FB}/s_L being between 1 and 2, suggesting that this may be a general trend within our modeling framework.

These results provide further confirmation of the significant role played by preferential diffusion in increasing the propensity for flashback when the hydrogen content is elevated. Moreover, we observe the crucial role of the slit width in influencing flame stabilization for high H_2 content.

Burner temperature. Fig. 12 shows the burner plate temperature map in the parameter space and the relative Sobol' indices. We note a strong dependency of T_B on the size of the slit, with wider slits resulting in higher temperatures. This is supported by the Sobol' index analysis, with I_W indicating a dependence of 71.7% on the slit width. Moreover, the interaction Sobol' index $I_{H_2,W}$ reveals that the variation of T_B within the investigated parameter range is not uniform: the maximum burner temperature, reaching approximately 1000 K, is observed in the region where $W = 1.2\,\text{mm}$ and %$H_2 \in [85\%, 90\%]$. Conversely, the minimum burner temperature of around 860 K is found in the region where %$H_2 = 100\%$ and $W = 0.5\,\text{mm}$.
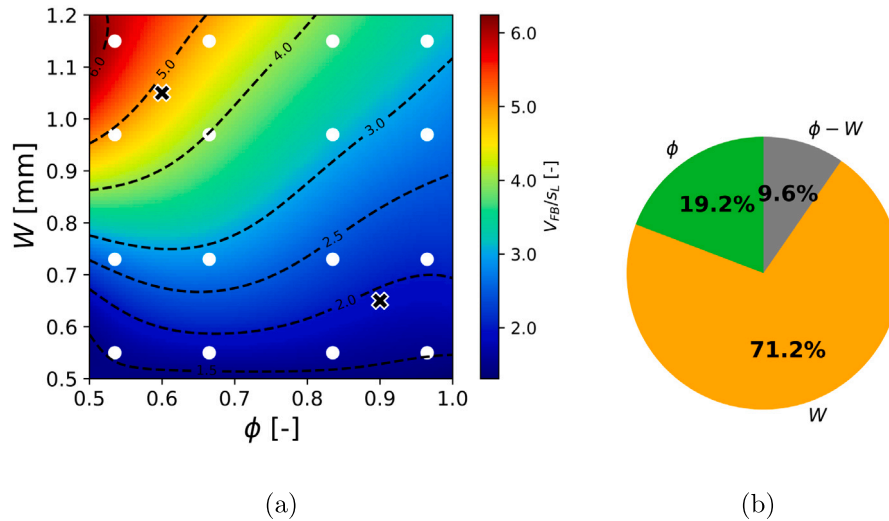
(a)

(b)

Fig. 14. (a) Stochastic response surface of V_{FB}/s_L in the ϕ - W parameter space. White dots represent quadrature points. Black crosses indicate test points. (b) Sobol' indices. (For interpretation of the references to color in this figure legend, the reader is referred to the web version of this article.)

It is important to note that in this study, increasing the slit width W corresponds to an increase in the distance D between two adjacent slits, to maintain a constant burner porosity. The work by Vance et al. [39] has demonstrated that changing the distance between the slits significantly impacts T_B by influencing the heat transfer mechanisms between the burner, the flame, and the burnt gases. As a result, the variations in geometry, combined with different mixture characteristics, lead to complex interactions that significantly impact the heat transfer processes and, consequently, non-trivially influence the temperature of the burner.

4.3. Effect of equivalence ratio and slit width

Finally, the stochastic sensitivity analysis is performed on the last pair of parameters, i.e., the equivalence ratio and the slit width, in the ranges $\phi \in [0.5, 1.0]$ and $W \in [0.5 \, mm, 1.2 \, mm]$, while fixing $\%H_2 = 100\%$. This specific value is chosen to maximize the sensibility to the parameters and due to its high practical significance. The test simulations are performed at the points corresponding to $\phi = 0.6$ and $W = 1.05 \, mm$, and $\phi = 0.9$ and $W = 0.65 \, mm$. Once again, the response surface values at these points align closely with the results from the test simulations, with an error margin of less than 2%.

Flashback velocity. In Fig. 13, we show the flashback velocity as a function of the two input parameters and the corresponding Sobol' indices. Even when keeping the H_2 content constant, a significant variability in V_{FB} is observed, ranging from approximately 1.0 m/s to 7.0 m/s. The primary parameter influencing this variability is W, as indicated by the Sobol' index $I_W = 66.4\%$. Additionally, ϕ contributes to the variation of V_{FB}, with a Sobol' index of 33.4%. Notably, the influence of these parameters on the flashback velocity is independent of each other, as indicated by the null interaction Sobol' index.

Normalized flashback velocity. Fig. 14 shows V_{FB}/s_L in the input parameters space and the relative Sobol' indices. Once again, significant variability is observed in the output quantity within the parameter space, with V_{FB}/s_L ranging from 1.2 to 6.1. The maximum value is observed for larger W and lower ϕ. The normalized flashback velocity is influenced by 71.2% by the slit width and by 19.2% by the equivalence ratio. Furthermore, the interaction Sobol' index indicates that the variability of V_{FB}/s_L is not uniform, with a higher impact when varying the slit width for low equivalence ratios (see Fig. 14).
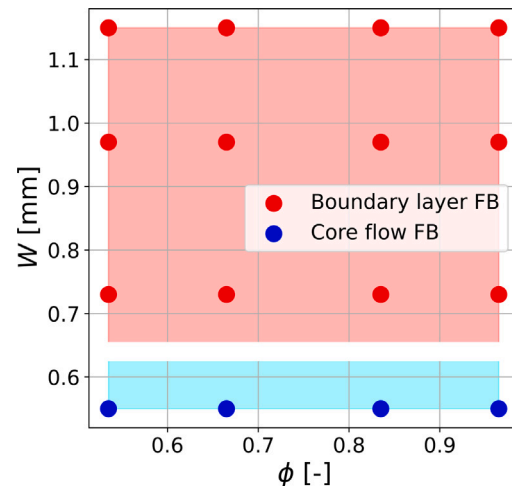

Fig. 15. Flashback regimes in the ϕ - W parameter space. Blue represents "core flow flashback", and red represents "boundary layer flashback". (For interpretation of the references to color in this figure legend, the reader is referred to the web version of this article.)

As expected from the previous analysis, which highlighted the influence of preferential diffusion effects on the relationship between V_{FB}/s_L and W, we observe a pronounced effect of the slit width, particularly for low equivalence ratios where preferential diffusion effects are more prominent. Another perspective is that the ratio V_{FB}/s_L exhibits a significant dependence on the equivalence ratio when the slit is sufficiently wide to allow preferential diffusion effects to play a crucial role. It is important to note that the extent of this influence may also vary depending on the chosen hydrogen content: in this case, being $\%H_2 = 100\%$, we assume that we are observing the maximum possible variability attributed to preferential diffusion effects. The division of the parameter space into "core flow flashback" and "boundary layer flashback" regimes is presented in Fig. 15. Again, it can be observed that the transition corresponds to values of V_{FB} between 1 and 2, reaffirming the universality of this phenomenon in our simulation context.

Burner temperature. The variation of the burner plate temperature T_B in the domain of interest is shown in Fig. 16 with the relative Sobol'
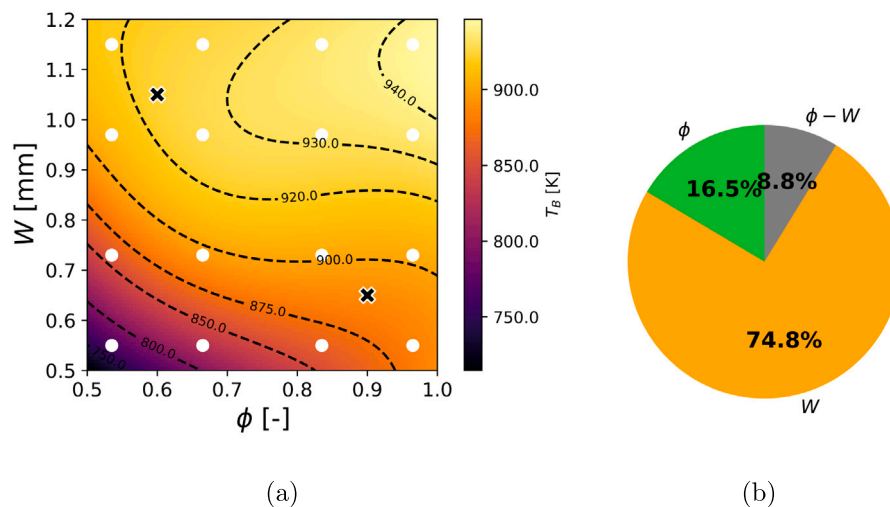
Fig. 16. (a) Stochastic response surface of T_B in the ϕ - W parameter space. White dots represent quadrature points. Black crosses indicate test points. (b) Sobol' indices. (For interpretation of the references to color in this figure legend, the reader is referred to the web version of this article.)

indices. We observe the burner temperature varying uniformly over the parameter space, with T_B increasing when increasing both ϕ and W. The Sobol' indices indicate a stronger dependence on W, being $I_W = 74.8\%$ and $I_\phi = 16.5\%$. We note that the burner plate temperature varies considerably on the domain, with an increase of ∼20% going from the lower-left corner ($T_B \simeq 760\,\mathrm{K}$) to the upper-right corner ($T_B \simeq 940\,\mathrm{K}$) in Fig. 16(a).

5. Conclusions

In this work, the use of gPC and stochastic sensitivity analysis has allowed us to gain a comprehensive and deep insight into the geometrical and operating parameters affecting the occurrence of flashback in perforated burners. The flashback velocity, V_{FB}, is primarily influenced by the H_2 content in the mixture. As the H_2 content increases, the flashback velocity also increases. However, as the mixture approaches 100% H_2, the effects of the equivalence ratio and the slit width become more significant, with V_{FB} decreasing with ϕ and increasing with W. It is important to note that the variability of V_{FB} is closely linked to the variability of the laminar flame speed s_L of the specific mixture under consideration. Therefore, V_{FB} may not provide a valid measure of the intrinsic flashback propensity of the mixture. To eliminate the dependence on the laminar flame speed, the normalized value of the flashback velocity, V_{FB}/s_L, is considered as a reliable indicator to evaluate the flashback propensity of a given parameter combination. Interestingly, regions in the parameter space that are more susceptible to preferential diffusion effects, such as high H_2 content and low equivalence ratio, exhibit higher values of V_{FB}/s_L. This is because preferential diffusion effects, particularly Soret-induced and curvature-induced preferential diffusion, play a significant role in flame stabilization. Furthermore, the slit width also plays a crucial role in determining the flashback propensity, especially when the hydrogen content is high or the equivalence ratio is low. All of the parameters under consideration exert an influence on the flashback dynamics, leading a transition between the "core flow flashback" and "boundary layer flashback" regimes as they are varied. Notably, this transition consistently occurs in the range of $V_{FB} \lesssim 1.5$ to $V_{FB} \gtrsim 2$. The burner temperature at the flashback limit, T_B, is mainly influenced by the burner geometry. Specifically, wider slits result in higher burner temperatures. The variability of T_B in the parameter space can be attributed to several factors, including the position of the flame at the flashback

limit, the total mass flow rate, radiative losses, the attachment of the flame to the burner plate, and the contact area between the hot burnt gases and the top surface of the burner plate. The aforementioned factors are dependent on both the specific geometry of the burner and the characteristics of the mixture, such as the adiabatic flame temperature, flame thickness, and Lewis number.

It is important to acknowledge that in practical devices, the burner temperatures can be affected by factors such as the finite size of the burners, necessitating potential corrections and adaptations of the model for real-world implementation. Furthermore, while our current model is based on a 2D representation, it is essential to consider that the three-dimensional structure of the slits could introduce significant variations in flashback dynamics, which may warrant further investigations. Nevertheless, our study sheds light on the complex interplay of various parameters and their interactions that influence the flashback propensity in high hydrogen content mixtures, with particular emphasis on the crucial role of preferential diffusion effects. In future works, further analyses could delve into understanding the relative impact of different sources of preferential diffusion on flashback velocity, including the Soret effect. The insights gained hold the potential for guiding the design and optimization of perforated burners, ensuring their safe and efficient operation in real-world applications. It should be noted that to achieve this, calibration and validation data from experiments, which are currently lacking, would be necessary.

CRediT authorship contribution statement

Filippo Fruzza: Writing – original draft, Methodology, Data curation, Conceptualization. **Rachele Lamioni:** Writing – original draft, Validation, Supervision, Methodology, Investigation, Data curation, Conceptualization. **Alessandro Mariotti:** Writing – review & editing, Methodology. **Maria Vittoria Salvetti:** Writing – review & editing, Methodology. **Chiara Galletti:** Writing – original draft, Methodology, Conceptualization.

Declaration of competing interest

The authors declare that they have no known competing financial interests or personal relationships that could have appeared to influence the work reported in this paper.

Data availability

The data that has been used is confidential.

References

[1] EU commission press release European green deal: the commission proposes transformation of EU economy and society to meet climate ambitions. 2021.

[2] REPowerEU: A plan to rapidly reduce dependence on Russian fossil fuels and fast forward the green transition. 2022.

[3] Quarton CJ, Samsatli S. Should we inject hydrogen into gas grids? Practicalities and whole-system value chain optimisation. Appl Energy 2020;275:115172. http://dx.doi.org/10.1016/j.apenergy.2020.115172.

[4] Mouli-Castillo J, Orr G, Thomas J, Hardy N, Crowther M, Haszeldine RS, Wheeldon M, McIntosh A. A comparative study of odorants for gas escape detection of natural gas and hydrogen. Int J Hydrogen Energy 2021;46(27):14881–93. http://dx.doi.org/10.1016/j.ijhydene.2021.01.211.

[5] Yang H, Lin X, Pan H, Geng S, Chen Z, Liu Y. Energy saving analysis and thermal performance evaluation of a hydrogen-enriched natural gas-fired condensing boiler. Int J Hydrogen Energy 2023. http://dx.doi.org/10.1016/j.ijhydene.2023.02.027.

[6] Younas M, Shafique S, Hafeez A, Javed F, Rehman F. An overview of hydrogen production: Current status, potential, and challenges. Fuel 2022;316:123317. http://dx.doi.org/10.1016/j.fuel.2022.123317.

[7] McKenna R, Bchini Q, Weinand J, Michaelis J, König S, Köppel W, Fichtner W. The future role of power-to-gas in the energy transition: Regional and local techno-economic analyses in Baden-Württemberg. Appl Energy 2018;212:386–400. http://dx.doi.org/10.1016/j.apenergy.2017.12.017.

[8] Michalski J, Bünger U, Crotogino F, Donadei S, Schneider G-S, Pregger T, Cao K-K, Heide D. Hydrogen generation by electrolysis and storage in salt caverns: Potentials, economics and systems aspects with regard to the german energy transition. Int J Hydrogen Energy 2017;42(19):13427–43. http://dx.doi.org/10.1016/j.ijhydene.2017.02.102.

[9] Smith C, Mouli-Castillo J, van der Horst D, Haszeldine S, Lane M. Towards a 100% hydrogen domestic gas network: Regulatory and commercial barriers to the first demonstrator project in the United Kingdom. Int J Hydrogen Energy 2022;47(55):23071–83. http://dx.doi.org/10.1016/j.ijhydene.2022.05.123.

[10] Zhao Y, McDonell V, Samuelsen S. Influence of hydrogen addition to pipeline natural gas on the combustion performance of a cooktop burner. Int J Hydrogen Energy 2019;44(23):12239–53. http://dx.doi.org/10.1016/j.ijhydene.2019.03.100.

[11] de Vries H, Levinsky HB. Flashback, burning velocities and hydrogen admixture: Domestic appliance approval, gas regulation and appliance development. Appl Energy 2020;259:114116. http://dx.doi.org/10.1016/j.apenergy.2019.114116.

[12] Wu X, Zhang H, Yang M, Jia W, Qiu Y, Lan L. From the perspective of new technology of blending hydrogen into natural gas pipelines transmission: Mechanism, experimental study, and suggestions for further work of hydrogen embrittlement in high-strength pipeline steels. Int J Hydrogen Energy 2022;47(12):8071–90. http://dx.doi.org/10.1016/j.ijhydene.2021.12.108.

[13] Kovač A, Paranos M, Marciuš D. Hydrogen in energy transition: A review. Int J Hydrogen Energy 2021;46(16):10016–35. http://dx.doi.org/10.1016/j.ijhydene.2020.11.256.

[14] A sustainable pathway for the European energy transition. In: Hydrogen roadmap Europe. 2019.

[15] Najarnikoo M, Targhi MZ, Pasdarshahri H. Experimental study on the flame stability and color characterization of cylindrical premixed perforated burner of condensing boiler by image processing method. Energy 2019;189:116130. http://dx.doi.org/10.1016/J.ENERGY.2019.116130.

[16] Lamioni R, Bronzoni C, Folli M, Tognotti L, Galletti C. Impact of H_2-enriched natural gas on pollutant emissions from domestic condensing boilers: numerical simulations of the combustion chamber. Int J Hydrogen Energy 2023. http://dx.doi.org/10.1016/j.ijhydene.2023.02.040.

[17] Lamioni R, Bronzoni C, Folli M, Tognotti L, Galletti C. Effect of slit pattern on the structure of premixed flames issuing from perforated burners in domestic condensing boilers. Combust Theory Model 2022. http://dx.doi.org/10.1080/13647830.2022.2157753.

[18] Schiro F, Stoppato A. Experimental investigation of emissions and flame stability for steel and metal fiber cylindrical premixed burners. Combust Sci Technol 2019;191(3):453–71. http://dx.doi.org/10.1080/00102202.2018.1500556.

[19] Edacheri Veetil J, Aravind B, Mohammad A, Kumar S, Velamati RK. Effect of hole pattern on the structure of small scale perforated plate burner flames. Fuel 2018;216:722–33. http://dx.doi.org/10.1016/J.FUEL.2017.12.057.

[20] Konnov A, Riemeijer R, de Goey L. Adiabatic laminar burning velocities of CH_4+H_2+air flames at low pressures. Fuel 2010;89(7):1392–6. http://dx.doi.org/10.1016/j.fuel.2009.11.002.

[21] Kurdyumov V, Fernández E, Liñán A. Flame flashback and propagation of premixed flames near a wall. Proc Combust Inst 2000;28(2):1883–9. http://dx.doi.org/10.1016/S0082-0784(00)80592-5.

[22] Su S-S, Hwang S-J, Lai W-H. On a porous medium combustor for hydrogen flame stabilization and operation. Int J Hydrogen Energy 2014;39(36):21307–16. http://dx.doi.org/10.1016/j.ijhydene.2014.10.059.

[23] Jiménez C, Fernández-Galisteo D, Kurdyumov VN. DNS study of the propagation and flashback conditions of lean hydrogen-air flames in narrow channels: Symmetric and non-symmetric solutions. Int J Hydrogen Energy 2015;40(36):12541–9. http://dx.doi.org/10.1016/j.ijhydene.2015.07.037.

[24] Zhang W, Wang J, Lin W, Mao R, Xia H, Zhang M, Huang Z. Effect of differential diffusion on turbulent lean premixed hydrogen enriched flames through structure analysis. Int J Hydrogen Energy 2020;45(18):10920–31. http://dx.doi.org/10.1016/j.ijhydene.2020.02.032.

[25] Kedia KS, Ghoniem AF. Mechanisms of stabilization and blowoff of a premixed flame downstream of a heat-conducting perforated plate. Combust Flame 2012;159(3):1055–69. http://dx.doi.org/10.1016/j.combustflame.2011.10.014.

[26] Vance F, Shoshin Y, van Oijen J, de Goey L. Effect of lewis number on premixed laminar lean-limit flames stabilized on a bluff body. Proc Combust Inst 2019;37(2):1663–72. http://dx.doi.org/10.1016/j.proci.2018.07.072.

[27] Vance FH, de Goey P, van Oijen JA. The effect of thermal diffusion on stabilization of premixed flames. Combust Flame 2020;216:45–57. http://dx.doi.org/10.1016/j.combustflame.2020.02.006.

[28] Wang Z, Han X, He Y, Wang S, Ji R, Zhu Y, Cen K. Investigation of flame and burner plate interaction during the heat flux method used for laminar burning velocity measurement. Fuel 2020;266:117051. http://dx.doi.org/10.1016/j.fuel.2020.117051.

[29] Jin W, Ren C, Li J, Wang J, Yan Y. Experimental study on characteristics of CH_4/H_2 oxy-fuel turbulent premixed flames. Fuel 2022;310:122292. http://dx.doi.org/10.1016/j.fuel.2021.122292.

[30] Kurdyumov V, Fernández-Tarrazo E, Truffaut J-M, Quinard J, Wangher A, Searby G. Experimental and numerical study of premixed flame flashback. Proc Combust Inst 2007;31(1):1275–82. http://dx.doi.org/10.1016/j.proci.2006.07.100.

[31] Kıymaz TB, Böncü E, Güleryüz D, Karaca M, Yılmaz B, Allouis C, İskender Gökalp. Numerical investigations on flashback dynamics of premixed methane-hydrogen-air laminar flames. Int J Hydrogen Energy 2022;47(59):25022–33. http://dx.doi.org/10.1016/j.ijhydene.2022.05.230.

[32] Xia H, Han W, Wei X, Zhang M, Wang J, Huang Z, Hasse C. Numerical investigation of boundary layer flashback of CH4/H2/air swirl flames under different thermal boundary conditions in a bluff-body swirl burner. Proc Combust Inst 2023;39(4):4541–51. http://dx.doi.org/10.1016/j.proci.2022.07.040.

[33] Ebi D, Clemens NT. Experimental investigation of upstream flame propagation during boundary layer flashback of swirl flames. Combust Flame 2016;168:39–52. http://dx.doi.org/10.1016/j.combustflame.2016.03.027.

[34] Ranjan R, Clemens NT. Insights into flashback-to-flameholding transition of hydrogen-rich stratified swirl flames. Proc Combust Inst 2021;38(4):6289–97. http://dx.doi.org/10.1016/j.proci.2020.06.017.

[35] Boulahlib M, Medaerts F, Boukhalfa M. Experimental study of a domestic boiler using hydrogen methane blend and fuel-rich staged combustion. Int J Hydrogen Energy 2021;46(75):37628–40. http://dx.doi.org/10.1016/j.ijhydene.2021.01.103.

[36] de Vries H, Mokhov AV, Levinsky HB. The impact of natural gas/hydrogen mixtures on the performance of end-use equipment: Interchangeability analysis for domestic appliances. Appl Energy 2017;208:1007–19. http://dx.doi.org/10.1016/j.apenergy.2017.09.049.

[37] Aniello A, Poinsot T, Selle L, Schuller T. Hydrogen substitution of natural-gas in premixed burners and implications for blow-off and flashback limits. Int J Hydrog Energy 2022. http://dx.doi.org/10.1016/j.ijhydene.2022.07.066.

[38] Pers H, Aniello A, Morisseau F, Schuller T. Autoignition-induced flashback in hydrogen-enriched laminar premixed burners. Int J Hydrogen Energy 2022. http://dx.doi.org/10.1016/j.ijhydene.2022.12.041.

[39] Vance F, de Goey L, van Oijen J. Development of a flashback correlation for burner-stabilized hydrogen-air premixed flames. Combust Flame 2022;112045. http://dx.doi.org/10.1016/j.combustflame.2022.112045.

[40] Fruzza F, Lamioni R, Tognotti L, Galletti C. Flashback of H_2-enriched premixed flames in perforated burners: Numerical prediction of critical velocity. Int J Hydrogen Energy 2023. http://dx.doi.org/10.1016/j.ijhydene.2023.04.252.

[41] Xiu D, Karniadakis GE. The Wiener–Askey polynomial chaos for stochastic differential equations. SIAM J Sci Comput 2002;24(2):619–44. http://dx.doi.org/10.1137/S1064827501387826.

[42] Goodwin DG, Moffat HK, Schoegl I, Speth RL, Weber BW. Cantera: An object-oriented software toolkit for chemical kinetics, thermodynamics, and transport processes. 2022, http://dx.doi.org/10.5281/zenodo.6387882, Version 2.6.0.

[43] Bilger R, Stårner S, Kee R. On reduced mechanisms for methane-air combustion in non-premixed flames. Combust Flame 1990;80(2):135–49. http://dx.doi.org/10.1016/0010-2180(90)90122-8.

[44] Ansys inc, Ansys fluent 22.1 user's guide. 2022.

[45] Stewart WE. Multicomponent mass transfer.. AIChE J 1995;41(1):202–3. http://dx.doi.org/10.1002/aic.690410124.

[46] Merk HJ. The macroscopic equations for simultaneous heat and mass transfer in isotropic, continuous and closed systems. Appl Sci Res, Sect A 1959;8(1):73–99. http://dx.doi.org/10.1007/BF00411741.

[47] Kuo K. Principles of combustion. Wiley; 2005.

[48] Modest MF. Chapter 17 - the method of discrete ordinates (SN-approximation). In: Modest MF, editor. Radiative heat transfer. third ed.. Boston: Academic Press; 2013, p. 541–84. http://dx.doi.org/10.1016/B978-0-12-386944-9.50017-0.

[49] Sobol' I. Global sensitivity indices for nonlinear mathematical models and their Monte Carlo estimates. Math Comput Simulation 2001;55(1):271–80. http://dx.doi.org/10.1016/S0378-4754(00)00270-6.

[50] Pope CJ, Shandross RA, Howard JB. Variation of equivalence ratio and element ratios with distance from burner in premixed one-dimensional flames. Combust Flame 1999;116(4):605–14. http://dx.doi.org/10.1016/S0010-2180(98)00062-5.